Journal of Cleaner Production 458 (2024) 142528

Contents lists available at ScienceDirect

Journal of Cleaner Production

journal homepage: www.elsevier.com/locate/jclepro

A multiscale examination of heat health risk inequality and its drivers in mega-urban agglomeration: A case study in the Yangtze River Delta, China

Hanyi Wu [a,b,c], Chuanwu Zhao [a,c], Yu Zhu [a,c], Yaozhong Pan [a,c,d,*]

[a] State Key Laboratory of Remote Sensing Science, Faculty of Geographical Science, Beijing Normal University, Beijing, 100875, China
[b] Beijing Engineering Research Center for Global Land Remote Sensing Products, Faculty of Geographical Science, Beijing Normal University, Beijing, 100875, China
[c] Key Laboratory of Environmental Change and Natural Disasters of Chinese Ministry of Education, Beijing Normal University, Beijing, 100875, China
[d] Academy of Plateau Science and Sustainability, Qinghai Normal University, Xining, 810016, China

ARTICLE INFO

Handling Editor: Cecilia Maria Villas Bôas de Almeida

Keywords:
Heat health risk assessment
Heat health inequality
Environmental justice
Multiscale
Yangtze River Delta

ABSTRACT

Increased frequency of extreme urban heat and its exposure to urban populations is one of the challenges presented by climate change, especially in urban clusters. Due to the rapid but unequal development, heat exposure disproportionately increased in the underdeveloped regions compared to the developed regions in urban agglomeration. To address this issue, it is crucial to clarify the spatial pattern of heat health risk (HHR) inequality for urban heat resilience. However, analyses for the disparity of HHR inequality often used a single scale, neglecting important spatial context effects at other scales. Moreover, the rationale of HHR inequality remains unclear. Here, we took the well-developed and highly urbanized Yangtze River Delta (YRD) region as a case study and employed multiscale approaches to examine how and why the HHR inequality varied at and within the regional scale. We first assessed HHR using a comprehensive assessment framework at a 1 km grid level. Then, we quantified the inequality between regions using local Moran's I and KS distance. Therefore, we utilized the Gini coefficient and Bayes quantile regression to quantify inequality and identify its drivers within the regional scale. Finally, we proposed a conceptual framework to inform policymaking in regions with different patterns of multiscale equality. Our results found that the HHR in YRD exhibited significant spatial inequality at the regional scale (Moran's $I = 0.562$, $P < 0.001$) and within the regional scale (Gini coefficient: 0.27–0.54). Higher population concentrations and building densities often led to higher HHR. In high HHR areas, intra-regional inequality was often lower due to high and coordinated socioeconomic levels (Gini coefficient: 0.27–0.34). Additionally, in areas with low and medium levels of risk, healthcare resource availability and local temperatures had a greater impact on intra-regional inequities, which varied at different levels of inequality. This study contributes to a better understanding of multiscale HHR inequality, which helps optimize heat risk management strategies and regional sustainable development.

List of abbreviations

BQR	bayes quantile regression
CI	confidence interval
DEM	digital elevation model
EHEs	extreme heat events
EVI	enhanced vegetation index
HHR	heat health risk
HRI	heat health risk index
HHI	heat hazard index
HEI	heat exposure index
HVI	heat vulnerability index
H/E/V	hazards/exposure/vulnerability
LST	land surface temperature
LULC	land-use and land-cover
MAUP	modifiable areal unit problem
NTL	nighttime light
Ta	near-surface air temperature
Tmax	daytime maximum Ta
Tmin	nighttime minimum Ta
YRD	Yangtze River Delta

(*continued on next column*)

(*continued*)

* Corresponding author at: No.19, Xinjiekouwai Street, Haidian District, Beijing, 100875, China.
E-mail addresses: hanyi.wu@mail.bnu.edu.cn (H. Wu), chuanwu@mail.bnu.edu.cn (C. Zhao), 202331051091@mail.bnu.edu.cn (Y. Zhu), pyz@bnu.edu.cn (Y. Pan).

https://doi.org/10.1016/j.jclepro.2024.142528
Received 27 December 2023; Received in revised form 26 April 2024; Accepted 8 May 2024
Available online 9 May 2024

1. Introduction

Climate change is causing an increase in global temperature, exacerbating the occurrence of more frequent and severe extreme heat events (EHEs) (Alizadeh et al., 2022; Hess, 2023). It has been demonstrated that intense and longer-lasting EHEs have become one of the deadliest natural hazards. The increasing EHEs have negative impacts on the heat-related health of urban residents, raising their heat health risk (HHR) (Mora et al., 2017; Venter et al., 2023; Wang et al., 2023). These impacts include impaired physical and mental health, human discomfort, and heat stress-driven diseases that can worsen cardiovascular, diabetic, and respiratory conditions (Estoque et al., 2020). Thus, it is critical to consider the population's heat-related health conditions, evaluate the HHR, and identify urban areas with high exposure to HHR for risk profiling, adaptation planning, and developing mitigation strategies. Therefore, an accurate and comprehensive characterization of the spatial distribution of heat health risk (HHR) and its multifaceted association with environmental and socioeconomic status is essential to protect residents' health and promote environmental justice in urban agglomerations.

HHR assessments are key to understanding urban heat and adaptation planning, providing spatial clarity on who, where, and to what extent is at risk (Ellena et al., 2023). This helps us to fully understand the different patterns of spatial distribution of HHR and helps decision-makers to develop appropriate strategies (Estoque et al., 2020; Wang et al., 2024). Previous researches are mainly based on the risk assessment framework in the Intergovernmental Panel on Climate Change (IPCC) Sixth Assessment Report (Parry, 2007; Pörtner et al., 2022), which quantitatively characterizes the spatial distribution of HHR in terms of hazard, exposure, and vulnerability. Recent studies have shown significant differences in residents' resilience and adaptability to extreme heat due to regional imbalances in development (Alizadeh et al., 2022; Venter et al., 2023). Spatial inequality results in varying HHR for populations in different regions, particularly in urban agglomerations with rapid and uneven development. This increased HHR is leading to a disproportionate burden of disease. Immediate action is required to decrease disparities in heat-related health risks and to establish health interventions at multiple levels, from the individual to the regional level, to curb this looming crisis (Fernández and Wu, 2016; Renteria et al., 2022).

Existing literature showed that HHR inequality is on the rise due to climate change, which is considered a significant environmental justice concern (Alizadeh et al., 2022), particularly in urban systems. Venter et al. (2023) found that individuals with lower incomes have less access to green space and are more vulnerable to heat, as evidenced by the spatial inequality of heat stress in Oslo, Norway. At the country scale, Alizadeh et al. (2022) demonstrated that heatwave exposure has disproportionately increased in the lowest-income regions compared to the highest-income regions. In addition, Lee H. et al. (2023) revealed that people outdoors, especially road workers are more susceptible to heat stress and face a high heat-related health risk due to the high radiation from concrete and asphalt roads from a local perspective. Similarly, Lee S. et al. (2023) investigated the relationship between perceived temperature and heat-related health risks considering the impact of concrete pavements. Although these studies have explored the inequality of HHR and the differences between their influencing factors, the analyses are often carried out using a single scale and drawing on readily available administrative spatial units, which can neglect the multiscale contextual correlations of risk inequality. In addition, spatial inequality and its effects cannot be fully understood by simply taking a single scale into account. Moreover, it is important to note that conclusions may vary depending on the scale of analysis. Petrović et al. (2022) have shown that the environmental risk analysis is often affected by the modifiable areal unit problem (MAUP), which highlights that different spatial scales capture different spatial processes. These findings raise the concern that a universal model and single-scale geospatial correlation index, such as geographically weighted regression (GWR) and Morans' I, which assume all processes operate at the same spatial scale, may not be appropriate in analyzing heat-related risk inequalities (Ho et al., 2015; Song et al., 2021). Additionally, previous research proposed that multiscale GWR and a combination of multiple scale geospatial correlation index allowed for the modeling of the effects of various variables, each of which varies at a specific spatial scale, simultaneously (Guan et al., 2023; Song et al., 2021). Conclusions based on the analysis of phenomena at a single spatial scale may not be spatially transferable, leading to potential misguidance in policymaking. Therefore, analyzing the inequality of risk at multiple spatial scales is necessary to provide accurate and reasonable references for local policymaking.

Some researchers analyzed the distribution of heat risk and its potential spatial influences on response and adaptation processes (Dialesandro et al., 2021; Ebi and Hess, 2020). They quantified the inequalities and made policy recommendations to promote regional HHR equality, improve urban resilience, and enhance resident well-being. For instance, Mohajerani et al. (2017) and KIM et al. (2019) pointed out that due to the relatively low albedo of AC compared to other pavement materials, AC pavements tend to have extremely high temperatures in summer climates and are considered to be a significant contributor to the urban heat island, which further contribute to the unequally spatial distribution of urban landscape heating, and the associated environmental and public health impacts (Beaudoin and Gosselin, 2016; Shamsaei et al., 2022). Wu et al. (2023) found that greenspace had multifaceted associations with heat stress in terms of inequality measures. Renteria et al. (2022) demonstrated that the inequality of HHR would increase with higher proportions of racial/ethnic minorities and people of lower socioeconomic status. However, the impact of the components of HHR itself, such as hazard, exposure, and vulnerability factors, on the unequal distribution of risk remains unclear, while no direct link has been established between these environmental and social influences and risk equality. In addition, urban agglomerations often have complex, multilevel, and nonlinear risk distributions (He et al., 2022; Mitchell and Chakraborty, 2015). Linking environmental and socioeconomic factors to the average equality level based solely on administrative boundaries at a single scale may lead to erroneous judgments. Previous studies have shown that the relationship between environmental justice and socioeconomic status varies depending on the level of equality (Guan et al., 2023; Sun et al., 2019). Therefore, it is necessary to investigate the impact of indicators on HHR equality at different quartiles of intra-regional equality levels in a multiscale context, considering multilevel differences within the urban agglomeration system.

In summary, previous studies have not analyzed HHR inequality from a multiscale perspective. To address this issue, it is critical to figure out the multiscale pattern of HHR inequality for urban heat resilience. Therefore, this study takes the well-developed and highly-urbanized Yangtze River Delta (YRD) as a case study and first examines the multiscale HHR inequality in such a mega-urban agglomeration at a 1 km grid level. Then, spatial autocorrelation and statistical methods are employed to interpret the relationship between HHR inequality and environmental and socioeconomic characteristics at and within the regional scale.

To better understand the spatial extent of HHR inequality, this paper considers multiple spatial scales, including macro, meso, and micro scales. It is important to note that these scales are not uniformly defined and must be contextualized within a specific scenario. In our case study on HHR in the YRD, we defined the macroscale as the regional and city scales. The districts and counties within the city were considered the mesoscale, and the micro-scale was defined as the smaller-scale units of communities and neighborhoods. At the macroscale, we quantified the inequality between regions using local Moran's I and KS distance. At the mesoscale, we utilized the Gini coefficient and Bayes quantile regression to quantify inequality and identify its drivers within the regional scale.

This study aims to investigate the environmental justice of HHR and its drivers in the YRD: (1) quantify the HHR and determine where heat health risk inequality may exist; (2) examine the multiscale HHR inequality based on spatial and statistical methods; and (3) explore the multifaceted associations between multiscale heat health risk inequality and environmental, demographic and socioeconomic characteristics to provide insights into urban environmental justice at both the regional and intra-regional scales from such a mega-urban agglomeration.

2. Materials and methods

2.1. Study region

The Yangtze River Delta is a vast metropolitan area located on the eastern coast of China (Fig. 1). It spans from 114.88°E to 122.83°E longitude and from 27.14°N to 35.13°N latitude, covering 358,000 square kilometers and encompassing 303 districts and counties in 41 cities. This region is one of the world's largest metropolitan areas, with a total population of 223.59 million people in 2017 (Zhong et al., 2017). The YRD urban agglomerations have undergone significant economic development and experienced tremendous growth in their urban population and urbanized areas due to rapid urbanization over the past several decades (Gao et al., 2023). It has played an important role in China's economic and social development.

The landscapes of YRD in the eastern and northern regions are plain landforms, while the south is characterized by hills. The YRD is mainly situated in the central subtropics and experiences a humid monsoon climate. The long-lasting influence of the West Pacific Subtropical High poses threats such as frequent extreme summer heat events in the YRD. In the context of climate change, urbanization is expected to increase the frequency of annual heat wave days in major metropolitan areas of the YRD, resulting in elevated levels of heat stress (Zhong et al., 2017). Recent studies have shown that urbanization and climate change have measurable effects on urban heat inequality (Todeschi et al., 2022; Wu et al., 2023). The large population and hot summers have led to serious heat-related health problems in this region.

2.2. Data and pre-processing

2.2.1. Geo-information data

To describe the heat hazard, meteorological observation data were obtained from the National Meteorological Data Center (http://data.cma.cn/data/weatherBk.html). These data were measured by automatic weather stations, comprising daily observation data from 269 stations in the YRD from June 1 to August 31, 2017, including daily near-surface maximum and minimum air temperatures (Ta). Additionally, the Moderate-resolution Imaging Spectroradiometer (MODIS) daily land surface temperature (LST) products (MOD11A1) with 1 km × 1 km (Wan et al., 2015), and ERA5 reanalysis data with 0.1° × 0.1° were collected (Copernicus Climate Change Service (C3S), 2017), which include the land surface skin temperature (T_{skin}), air temperature at the 2-m altitude (T2m), soil temperature (STL), wind speed at the 10-m altitude and surface pressure (SUP). Furthermore, we performed the filling of missing MODIS LST values based on machine learning approaches, using the relevant auxiliary variables such as T_{skin} from ERA5 as the independent variable and the high-quality LST acquired under clear sky condition as the dependent variable (more details were provided in supplementary material).

Two auxiliary data, the digital elevation model (DEM) and land-use and land-cover (LULC) were also collected from the Advanced Spaceborne Thermal Emission and Reflection Radiometer (ASTER) (NASA/METI/AIST/Japan Spacesystems And U.S./Japan ASTER Science Team, 2009) and Finer-Resolution Observation and Monitoring of the Global Land Cover (FROM-GLC) project (Gong et al., 2013), respectively.

To obtain a more accurate exposure indicator, MODIS enhanced vegetation index data (EVI) (Didan, 2015) and VIIRS Nighttime light (NTL) data (Román et al., 2018) were collected and then a population spatialization method was used to obtain gridded population density with 1 km × 1 km based on NTL data and auxiliary data.

Road network data and healthcare points of interest (POI) data were collected from Open Street Map (OSM) and Amap (lbs.amap.com), respectively. The availability of medical resources was measured using the cumulative distance tool in ArcGIS software.

2.2.2. Statistical data

The study also obtained county-level socioeconomic data from the

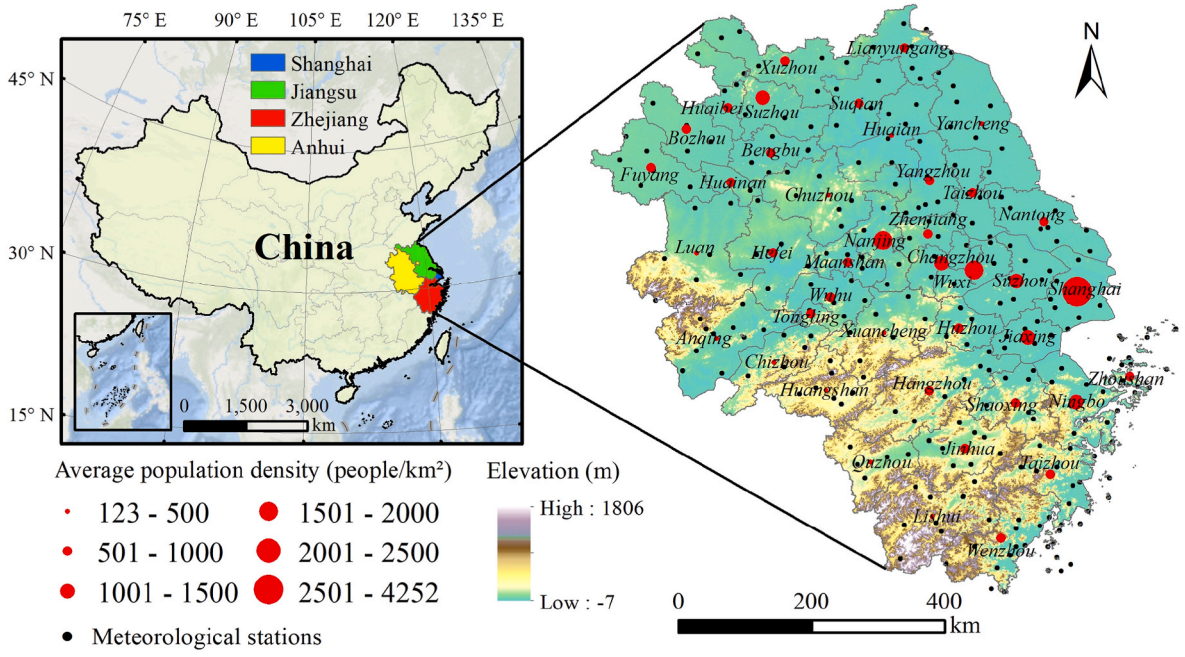

Fig. 1. Study region.

2017 statistical yearbooks of Shanghai, Zhejiang, and Jiangsu provinces, as well as some local statistical bureaus. The data include the resident population, proportion of elderly population, number of healthcare facilities beds, government budget revenue, disposable income, and GDP per capita of the 303 districts and counties in the YRD.

More details regarding the data processing can be seen in the Data Section in the supplementary materials.

2.3. Heat health risk assessment

The effects of climate extremes on individuals depend on the severity of the extremes, as well as their exposure and vulnerability. To comprehensively assess the risk of heat-related health issues, we utilized the conceptual framework proposed by the IPCC (Parry, 2007; Pörtner et al., 2022) to combine heat hazards (H), human exposure (E), and vulnerability (V) factors. Therefore, the Heat Health Risk Index (HRI) was calculated by multiplying three equally weighted risk components to quantify the HHR (Cutter and Susan, 2006; Estoque et al., 2020; Koks et al., 2015; Wang et al., 2023), as shown in Eq. (1). The spatial distributions of the three factors were mapped and analyzed at the 1 km grid level. The overlap of these three factors for urban heat health risk allows for the identification of pixels with a high level of risk (see Fig. 2).

$$HRI = HHI \times HEI \times HVI \quad (1)$$

where HRI, HHI, HEI, and HVI represent the heat health risk index, the heat hazard index, the heat exposure index, and the heat vulnerability index, respectively.

All the indicators subcategorized in H, E, and V factors were first positively transformed and Z-score standardized into the range of 0–1, and then combined to derive HHI, HEI, and HVI based on subjective (expert score) and objective weight (entropy weight), respectively.

2.3.1. Hazard

Heat hazard refers to the distribution of hazards resulting from EHEs that may cause loss of life, injury, or other health impacts. To measure the human perception of heat more appropriately, heat hazard was represented as the retrieved near-surface air temperature, which was obtained based on the meteorological observation station data, the gap-filled LST data, and related auxiliary data. Machine learning methods, specifically gradient boosting decision tree (GBDT), RF, and eXtreme Gradient Boosting (XGBOOST) models, were chosen for modeling. The dependent variables were the daytime maximum Ta (T_{max}) and nighttime minimum Ta (T_{min}) from meteorological station data, while the independent variables included gap-filled LST, EVI, elevation, and SUP from MODIS, ASTER DEM, and ERA5 products. The optimal models applied to retrieve daily T_{max} and T_{min} were selected based on ten-fold cross-validation and the coefficient of determination (R^2). Based on the retrieved air temperature, a hot day is defined as a day with a T_{max} greater than 35 °C, and a heat wave event is defined as defined as an extreme heat event with T_{max} over 35 °C for 3 or more consecutive days. To quantify the heat hazard, the following four indicators: *(i)* daily T_{max}, (ii) daily T_{min}, *(iii)* The number of hot days, and *(iv)* the frequency of heat wave events were selected. (more details were provided in the Data and Method Section of supplementary material).

2.3.2. Exposure

Human exposure refers to the presence of people who are likely to be adversely affected by EHEs and their living environment during the hazards. In this regard, we used both population density and vegetation coverage (EVI) as indicators of exposure given that both have been widely used in existing studies (Huang et al., 2023; Wu et al., 2024). In addition, to obtain gridded population density, a model was developed first using NTL, LULC, and auxiliary data as input variables to estimate

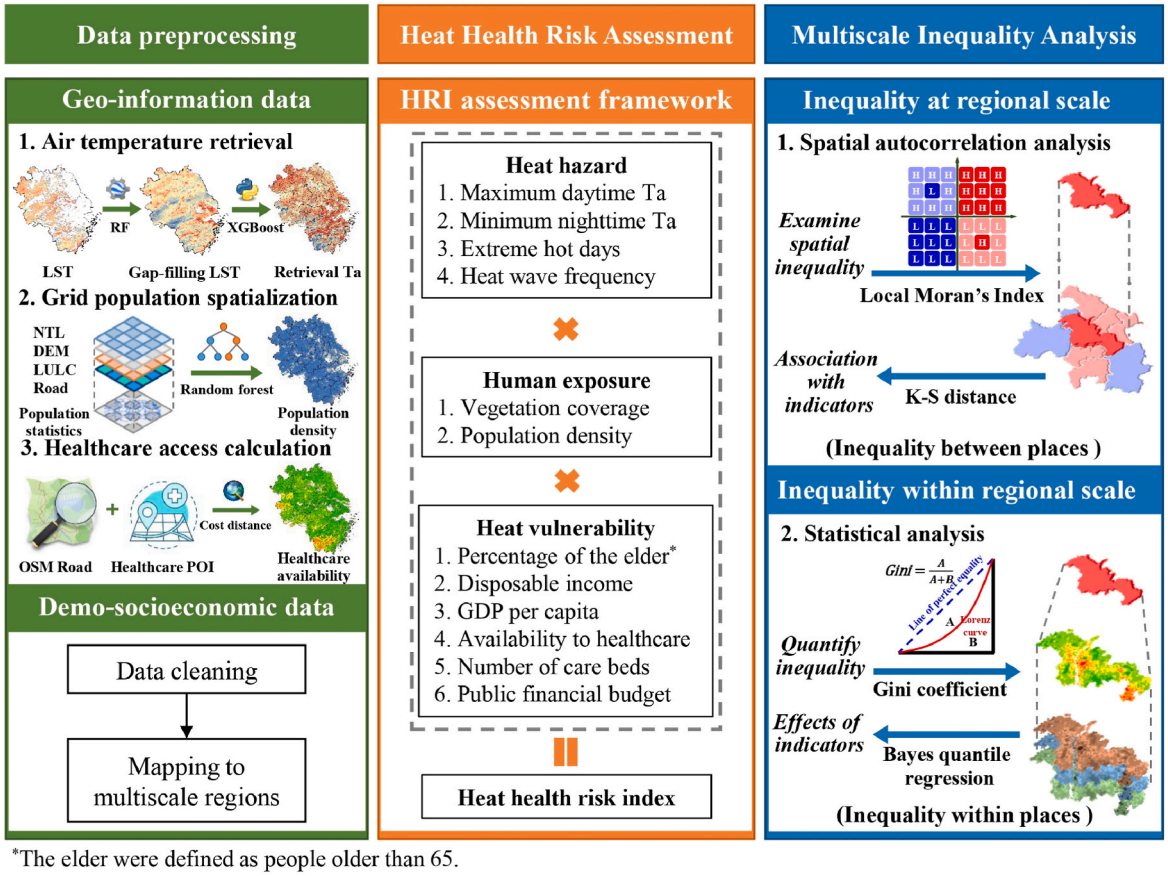

*The elder were defined as people older than 65.

Fig. 2. Technical flowchart.

the county-level population density. The fitted model was then applied to the 1 km spatial variables to spatialize the population density. The estimated gridded population density was corrected based on statistical data to ensure consistency with the statistical population at the county level (more details were provided in the supplementary material).

2.3.3. Vulnerability

Heat vulnerability refers to the capacity of hazard-affected populations to cope with the hazard and their sensitivity or susceptibility to harm. Six indicators derived from socioeconomic and demographic statistics were utilized to measure vulnerability: (i) elderly population (Huang et al., 2023; Zhu and Yuan, 2023), (ii) socioeconomic status (Burke et al., 2015; Sun et al., 2022), (iii) income (Adams et al., 2022; Wu et al., 2024), (iv) medical resource condition (He et al., 2019; Zhang et al., 2019), (v) infrastructure condition (Ellena et al., 2023; Inostroza et al., 2016), and (vi) governance capacity (Cheng et al., 2021; Niu et al., 2021). The elderly population was defined as the percentage of people 65 years of age or older. The socioeconomic status and income were quantified by the GDP per capita and the disposable income of residents, respectively. Medical resource condition refers to the availability of medical resources, which is measured by the cost of walking time to the nearest medical site. The infrastructure condition and governance capacity were quantified as the number of beds in public health facilities and public financial budget revenue, respectively.

More details of the indicator selection and process can be seen in the Data and Method Section in the supplementary materials.

2.4. Examining the HHR inequality at the regional scale

We employed both spatial and statistical methods to analyze the spatial distribution of HHR inequality and explore its multifaceted association with the 12 indicators used in the HHR assessment framework.

First, to examine the differing distributions of HHR inequality, we used a local analysis to explain the presence of similar neighborhoods. We employed univariate local Moran's I, which is an effective method for detecting the hot spots or cluster areas of environmental exposure inequality based on spatial autocorrelation theory. This helped us determine the local spatial distribution of hot spot and cold spot areas of mean HRI values at a regional scale. Moran's I index calculates the difference between the target and the mean for all values, with a range between −1 and 1 (Mitchell and Chakraborty, 2015; Wong et al., 2016). A positive value indicates that spatial objects have similar neighbors (i.e., high values near high values; low values near low values), while a negative value indicates the opposite. If the values tend to be random spatially, the index will be near zero. Therefore, we considered 'High--high' areas to be high-risk areas of spatial inequality.

Second, to explore the relationship between HHR inequality and the environmental and socioeconomic indicators, we considered the HRI into five inequality levels based on the spatial autocorrelation result: High-high (HH), High-Low (HL), No significance (No Sig.), Low-high (LH) and Low-Low (LL). We then used the Kolmogorov-Smirnov (KS) distance (Justel et al., 1997) to assess the variation of selected indicators across different levels. To measure sensitivity between different levels, we utilized this non-parametric statistical test. The K–S distance, which measures the sensitivity of differences in both the location and shape of data distributions (Langlois et al., 2012; Pianosi and Wagener, 2015), is used to indicate the similarity or difference of indicators across different inequality HRI levels and reveal the multifaceted association among them.

2.5. Deriving the HHR inequality-indicators relationship within the regional scale

In this section, we quantified the HHR inequality with the Gini coefficient and examined the quantile effect of environmental and socioeconomic status on HHR inequality.

An inequality analysis of YRD within the regional scale was conducted, considering temperature characteristics, environment, demographic, and socioeconomic characteristics. The Gini coefficient (Dorfman, 1979) was calculated to quantify the inequality level of each subregion in the study area. The spatial Gini coefficient quantifies the curve distribution of HRI in a spatially explicit way. The Gini Index ranges from 0 (representing total equality) to 1 (representing total inequality), as shown in the Eq. (2):

$$G = 1 - \sum (q_i + q_{i-1})(p_i - p_{i-1}),\ q_i = \sum_{j=1}^{i} y_j \Big/ \sum_{j=1}^{n} y_j,\ p_i = i \Big/ n \qquad (2)$$

Where i is an accumulative counter that counts by 1 from zero to n. q_i is the cumulative proportion of one selected indicator at count i over the sum of that indicator of all raster pixels. p_i is the cumulative proportion of areas over all areas at count i. n is the total number of raster pixels within the regional scale.

Second, we applied Bayes Quantile Regression (BQR) to investigate the effects of HRI indicators on its equality and how these effects vary based on the level of spatial equality within regional scales. This analysis would reveal the cross-scale pattern of HHR inequality. In contrast, the classic ordinary least squares (OLS) regression only estimates the effect of the HRI spatial pattern on its equality at the average level, which may be biased by extreme values (Xu et al., 2019). Compared with OLS, BQR does not assume normality and allows the covariates to affect the entire conditional distribution rather than just the mean (Guan et al., 2023). This approach was used to assess the robustness of environmental research outcomes to changes in environmental exposure levels (Xu et al., 2019). The underlying assumption is that the effects of HRI indicators differ between areas with relatively equal HHR distribution and those with extreme HHR disparity. It is necessary to note that BQR results do not provide p-values to indicate significance and the significance of a variable depends on whether the distribution of coefficients within the confidence interval (CI) contains 0. So, we performed 5000 iterations using the 'bayesQR' package in RStudio, removing the first 100 iterations for stability and accuracy. Therefore, we used box plots of the coefficients to determine the significance of the relationship between the indicators and equality. Our model for the BQR analysis is shown in Eq. (3):

$$Y_i = \alpha_1^p x_1 + \alpha_2^p x_2 + \alpha_3^p x_3 + \cdots + \alpha_n^p x_n + e \qquad (3)$$

Where the dependent variable Y_i is the Gini coefficient that represents HHR equality within each regional unit; the independent variable x_n includes all indicators employed in HRI assessment, α_n^p is the variable coefficient at the pth quantile, and e is the error term.

3. Result

To examine the multiscale spatial inequality of HHR, as quantified by HRI values in the results, we start by displaying the spatial distribution with the smallest available scale (1km × 1 km grid cells). We then introduce other scales to gain insight into how these various spatial patterns differ in terms of HRI and inequality levels and to demonstrate the impact of spatial scale on measuring inequality. Finally, we present the cross-scale patterns of the spatial inequality of HRI in the YRD.

3.1. Spatial distribution of heat health risk and its components

To provide an understanding of the spatial difference of the values at the pixel level, (a) heat hazard (b) human exposure (c) heat vulnerability, and (d) the heat health risk index were produced, which were divided into 5 levels ranging from 'Low (L)' to 'High (H)' by Jenk natural break method.

The heat hazard map (Fig. 3(a)) depicts the fragmented distribution of heat hazards. Considerable differences in the HHI spatial pattern were

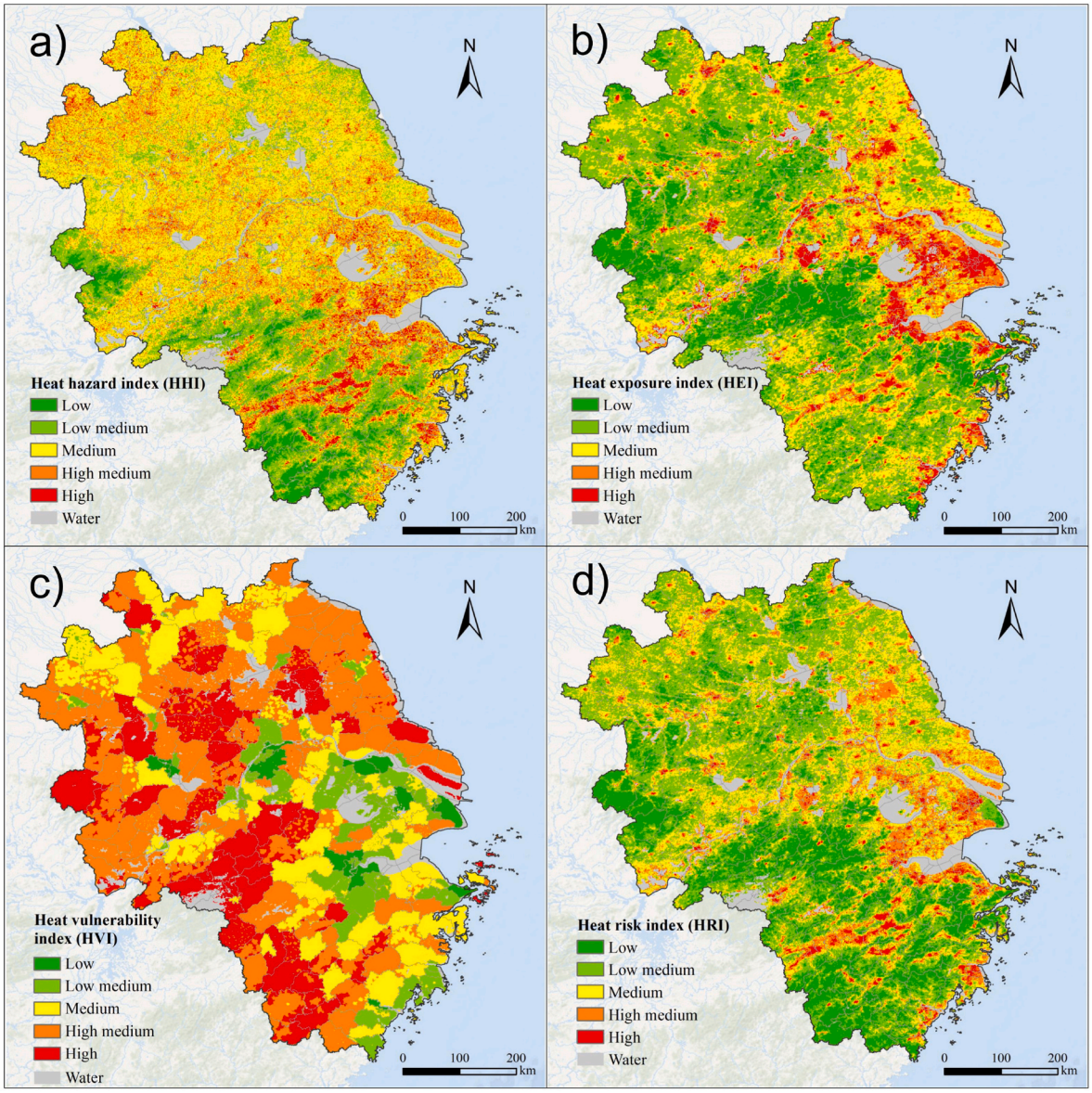

Fig. 3. Spatial distribution of the heat health risk factors and index in the YRD. (a) heat hazard index; (b) heat exposure index; (c) heat vulnerability index; (d) heat risk index.

observed. The coast of Hangzhou Bay had the highest HHI values, which corresponded to higher impervious surface levels. Conversely, the southwestern region of YRD had the lowest values. Additionally, Fig. 3 (b) illustrated the distribution of human exposure based on population density and vegetation coverage, which was non-uniform and easily interpretable. City centers often have higher levels of exposure due to their high population density and lower vegetation coverage. Furthermore, Fig. 3(c) displays the spatial distribution of vulnerability factors in the YRD. To some extent, socioeconomic status could indicate the adaptability and resilience of residents to HHR. Due to the significant socioeconomic development gap between the western and eastern regions, the western YRD region was highly vulnerable.

The spatial pattern of the heat risk index in YRD is presented in Fig. 3 (d), revealing significant spatial variation. The Shanghai-centered urban agglomeration, urban cities along with Hangzhou Bay (e.g. Hangzhou and Ningbo) and the prefecture-level urban areas of Jiangsu (e.g. Nanjing and Suzhou), Zhejiang (e.g. Taizhou and Wenzhou), and Anhui (e.g. Hefei and Wuhu) provinces had the highest HRI levels, which was attributed to high heat hazards and exposure. These metropolitan areas had high levels of HRI due to the concentration of urban development and high population density resulting from rapid urbanization. Additionally, the high HRI areas in the Jin-qu basin of Zhejiang were influenced by specific topography, continuous hot weather, and poor socioeconomic status. In contrast, the central and southern regions of the YRD, which were primarily covered by forests and crops, were mainly low-risk areas. These areas were also affected by topography, land use, and sparse populations.

3.2. *Inequality between places*

The spatial distribution analysis of the HRI 'hot spots' and 'cold spots' revealed interesting patterns in the YRD. In Fig. 4, significant clustering of high HRI value areas was presented in the Shanghai-centered urban agglomeration, while low-risk areas were found in the western, middle, and southern parts of YRD (Moran's $I = 0.562$, $P < 0.001$). These regions and their distinct clustering may indicate suburban sprawl and densification of the impervious landscape.

However, there were regional areas of high urban heat risk outliers that were surrounded by neighborhoods exhibiting lower urban heat risk. Identifying outliers presented a similar composition related to the

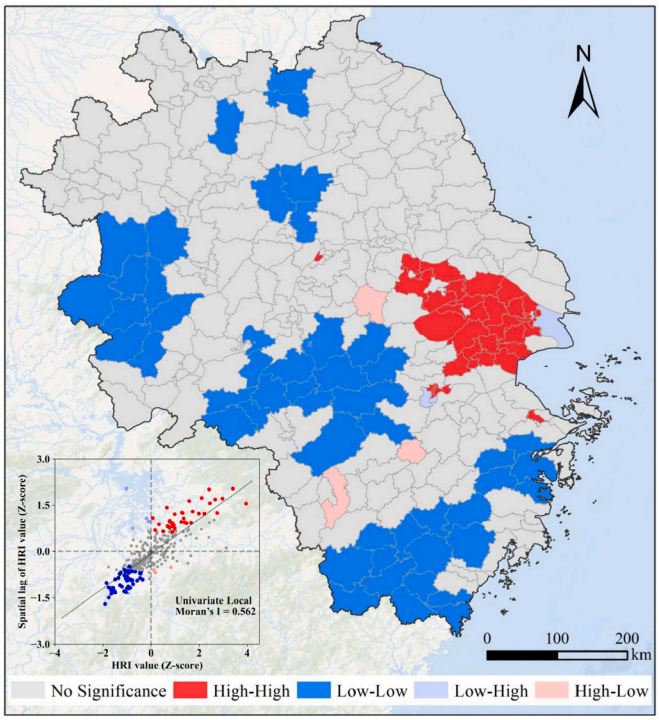

Fig. 4. Spatial distribution of HRI cluster type measured by local Moran's I (e.g. High-High means high-value clustering areas and Low-High means that outliers with low values are surrounded by high values.

relatively denser built environment landscape, higher levels of urbanization, and population concentration than surrounding cities at a regional scale. These spatial outliers of high urban heat risk existed in the city centers of Jinhua (in the mid-west of Zhejiang Province), Quzhou (in the west of Zhejiang Province), and Changzhou (in the southwest of Jiangsu Province), which were rendered as pink in Fig. 4.

In addition to the local Moran' I, which measured the spatial distribution of HHR inequality at a regional scale, the KS-distance statistics examined the variation across different areas of regional inequality. This interpretation could explain why HHR inequality shows the pattern in Fig. 4. The KS-distance matrix patterns suggested that certain indicators, including maximum and minimum temperatures, the number of extremely hot days, the frequency of heatwaves, and the availability of medical resources (Fig. 5 a-d, k), had less KS-distance value and less dissimilarity compared to the other indicators. Apart from this shared pattern, minimum temperature and availability of medical resources in HH areas differed considerably from LL areas (KS-distance = 0.64, $p < 0.001$ and KS-distance = 0.48, $p < 0.001$).

On the other hand, the exposure indicators and the other vulnerability indicators showed higher dissimilarity overall. For instance, at the bottom of the matrix of Fig. 5(g), the elder ratio indicator in the LL heat risk areas differed significantly from that in the HL heat risk areas (KS-distance = 0.46; $p < 0.001$), and this difference was shown as the risk level increases (from 0.6 to 0.84; $p < 0.001$). In addition to this, the indicator for GDP and number of care beds (Fig. 5 h-j) in the HL level heat risk areas were more distinct from those in the other level heat risk areas, which were located in the city center of Jinhua and Quzhou city. The spatial pattern suggested that both GDP and the number of care beds were concentrated in the city center, with less concentration in suburban areas, in the context of these two developing cities with poor economic conditions. This concentration partly contributed to a high HRI value surrounded by a low HRI value and a high KS distance between the HL level and other levels.

3.3. Inequality within places

The Gini coefficient ranged from 0.27 to 0.54, indicating an uneven distribution of HRI in the YRD. Half of the Gini coefficients were in the fourth quantile, indicating highly unequal HRI distribution in almost half of the areas within the regional scale. Fig. 6 showed the spatial distribution of the Gini coefficient. It revealed that the HRI distribution within regional units in the southwest YRD districts is extremely uneven, while the northeast YRD districts were comparatively more equal. Compared with Fig. 4, we could find that the unequal area located in the southwest YRD tends to have low HRI values within the regional scale, while the comparatively more equal area has higher HRI values, inversely. It could be explained in pixel level HRI map (Fig. 3(d)) that high HRI area equally emerged with high-level HRI both in the urban and suburban due to high-density building environment and cluster population at regional scale, with low intra-regional inequality. However, in developing areas such as Jinhua and Quzhou cities, where the socioeconomic level was relatively underdeveloped, the population and social resources were mainly concentrated in central urban areas. Despite a relatively low level of risk, this concentration led to significant intra-regional inequalities.

The correlation between HRI indicators and the Gini coefficient varied at different equality levels (Fig. 7). Regarding hazard indicators, daytime maximum temperature had a negative effect on the Gini coefficient at the 0.5 quantile and a little positive tendency at 0.25 and 0.75 quantile; while nighttime minimum temperature had a negative effect on the Gini coefficient at the 0.25 quantile and 0.5 quantile. However, this effect lost its significance at the 0.75 quantile. The nighttime minimum temperature only significantly improved equality in areas with a higher equality level. Therefore, the number of extremely hot days and heat waves were not significantly correlated with HRI equality. Regarding exposure indicators, population density exhibited a negative trend across all quantiles, while the EVI showed a positive tendency on HRI intra-regional inequality. For vulnerability indicators, all socioeconomic indicators were not significantly correlated with HRI equality except the public health-related indicators. The availability of healthcare had a significantly positive effect on the Gini coefficient at the 0.5 quantile and a positive tendency at the 0.25 quantile. This indicated that residents in medium-level intra-regional equality areas tended to have less equal availability of healthcare facilities. Furthermore, the number of care beds had a negative tendency at 0.5 and 0.75 quantile but did not show any obvious effects on the Gini coefficient at 0.25 quantile.

3.4. Cross-scale patterns of HHR spatial inequality

To compare different spatial contexts and explore the rationale of the cross-scale pattern of HHR inequality, we decomposed the comparison of the Gini index into the within-profile (cross-scale) inequality (Fig. 8), which compared the intra-regional inequality in the context of regional inequality. In different HRI clustered areas, there was huge spatial inequality between areas, which could be reclassified into three clustered types according to Section 3.2, consisting of low level (LL and HL), medium level (No significance), and high level (LH and HH). In these three HRI levels, the availability of healthcare was the most significant indicator among all. In the medium-level areas, the availability of healthcare had a significant positive effect on the Gini coefficient at 0.75 quantile and a positive tendency at 0.25 quantile. In the low-level areas, the effects of the availability of healthcare were only significantly negative at 0.5 quantile. It indicated the increase in the availability of healthcare can improve HRI equality within a regional scale with medium equality and low HRI levels but might not be as effective as that in less equal and higher HRI areas.

The maximum temperature had a negative tendency on intra-regional inequality in medium and high HRI level areas at 0.25 quantile but had a positive tendency at 0.5 quantile in low HRI level areas. This means areas with higher temperatures indicated more equally

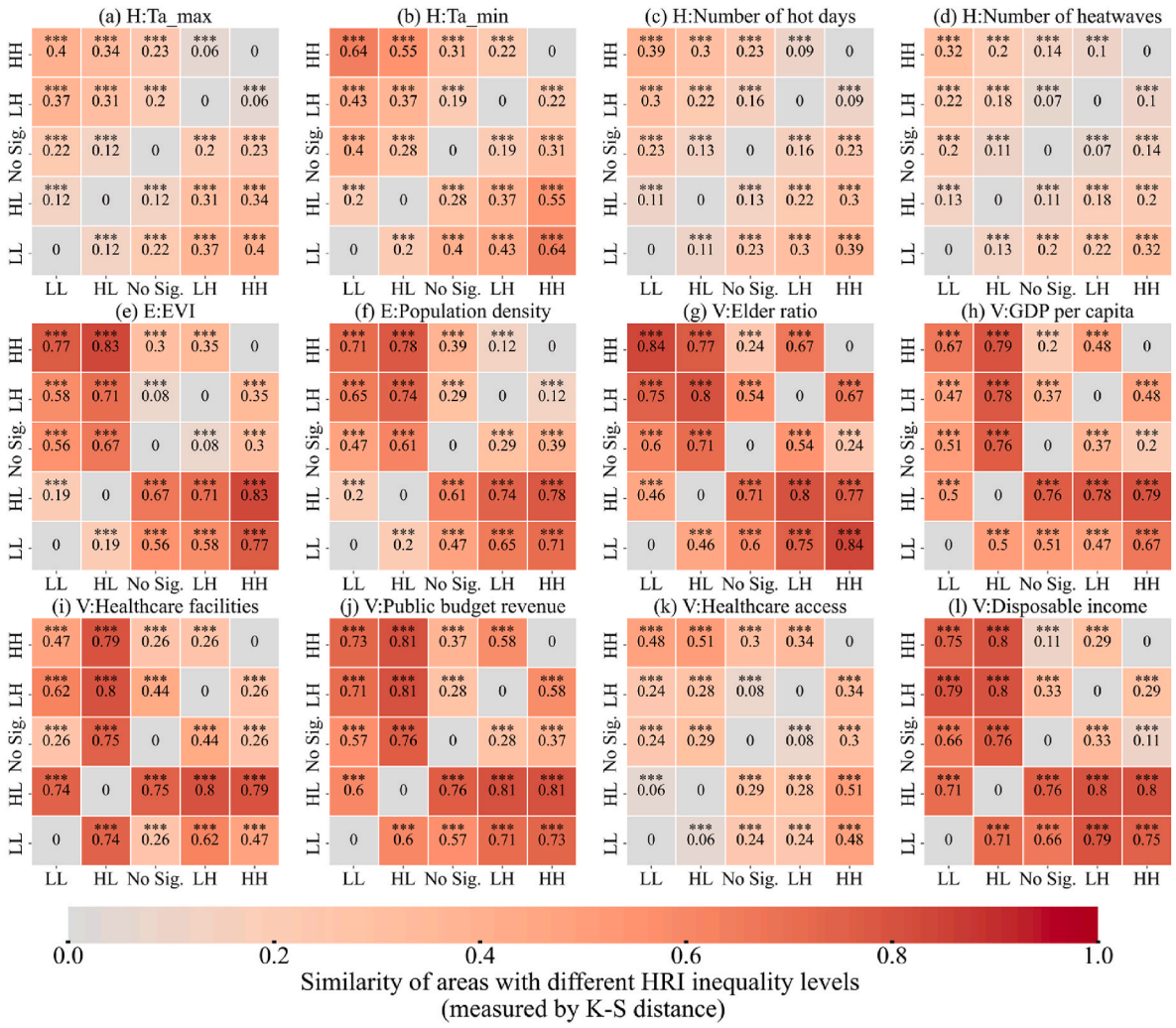

Fig. 5. The heat map shows the similarity of area with different inequality levels (measured by K–S distance) of all normalized indicators. The farther the K–S distance is, the more dissimilar the area with different HRI levels is.

distributed in higher HRI level areas but unequally distributed in low HRI level areas. However, the minimum temperature only had a little positive effect on the Gini coefficient in high HRI areas. Though not significant, the other indicators tended to have the same distribution pattern. The distribution of coefficients was more decentralized in low and high HRI level areas while more centralized in medium areas. It was indicated that these indicators had more possibility to influence the HRI intra-regional equality in low and high HRI areas than in medium-level areas.

4. Discussion

4.1. Spatial inequality in HHR: the issue of spatial scale

In this study, we qualified the HHR and analyzed its multiscale spatial inequality between and within places. We employed the local Moran's I and Gini coefficient to measure multiscale inequality in HHR at regional and intra-regional scales based on the results of the HHR quantification at a 1-km grid level. The results indicated that the measurement of equality in HHR was greatly affected by scale, which in turn affects the analysis and comparison across regions. To understand HHR and the environmental injustice it causes, it is critical to make multiscale comparisons within and across regions. Policy responses to heat stress should not rely solely on regional-scale definitions while ignoring inequalities within individual cities. In addition to intra-city inequalities, there are also considerable inequalities between cities, and policy responses need to be contextualized (Petrović et al., 2022). Our work explicitly examined HHR and fostered the multifaceted association between indicators and multiscale HHR inequality.

4.2. Effects of risk indicators on HHR

The urban agglomeration with high HHI surrounding Shanghai experiences the highest temperatures, which is due to the high degree of urbanization and the urban heat island effect (Supplementary Fig. S7 (a)). The spatial distribution of heat waves is also heavily influenced by climatic conditions affected by subtropical high pressure in southern YRD. This area experiences the highest number of extremely hot days and the most frequent heat waves, up to 10 times during summer (Supplementary Figs. S7(c–d)), which contributed to the regional inequality of heat hazard and even the HHR.

Additionally, a significant correlation is observed between vegetation distribution and urbanization levels (Supplementary Fig. S8). It is indicated that areas with high levels of urbanization have dense impervious surfaces and sparse vegetation, resulting in a low vegetation index. The areas with low vegetation index were concentrated in the Shanghai-centered urban agglomeration, which could typically characterize the underlying environmental conditions. This metropolitan area exhibits higher exposure to EHEs due to the high-level urbanization and population agglomeration, which was the main contributor to the

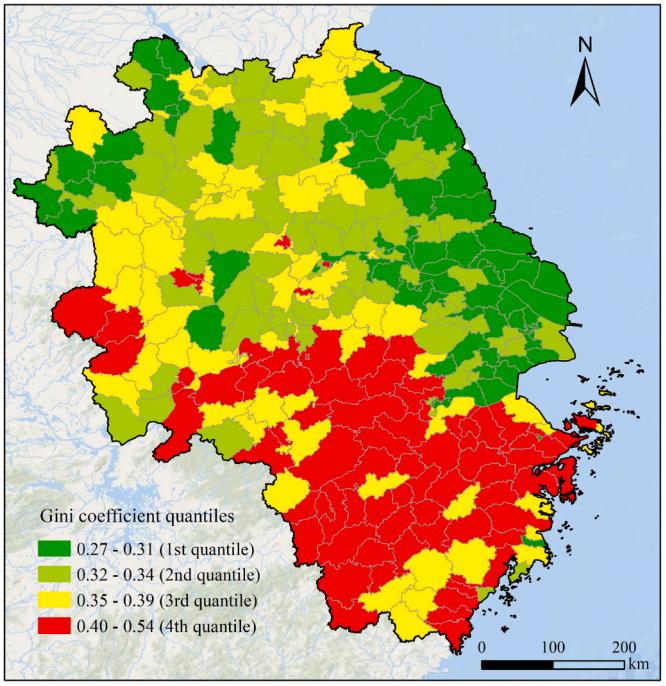

Fig. 6. Spatial distribution of the Gini coefficient (This figure shows the Gini coefficient for each district in our study area. From red to green, the Gini coefficient decreases, and the equality level of heat health risk increases). (For interpretation of the references to colour in this figure legend, the reader is referred to the Web version of this article.)

regional and intro-regional inequality of HHR as well.

Furthermore, the distribution of vulnerability indicators also had a significant impact on HHR at the regional scale (Supplementary Fig. S9). From the perspective of income and GDP, the high-value areas are on the developed southeast coast. Conversely, the areas with poor economic conditions are the northwest of Anhui Province. It demonstrated that the socio-economic characteristics were seriously polarized and regional development was uneven and unequal. In addition, the overall trend of the public financial budget shows a decreasing trend from the east to the west. Therefore, a quarter of the YRD has a high proportion of the aged population, including southern Jiangsu and Shanghai. As for medical resource conditions, the Shanghai urban agglomeration was characterized by an abundance of medical resources, a highly developed medical level, and high accessibility. Medical resources have a stronger correlation with the local economic status and awareness of the importance of public healthcare than with economic-related indicators.

4.3. The multiscale HHR inequality and environmental injustice

Spatial measures and statistical analyses can reveal inequalities between and within regions at multiple scales, exposing a complex spatial structure within mega-urban agglomeration. For instance, at the meso-scale, Shanghai has a high concentration of risk, while at the macro-scale, there is no significant risk inequality within the city. In contrast, the western YRD exhibits high-risk inequality at the intra-regional scale in areas such as Huangshan City and Lishui City due to their concentration of population and socioeconomic resources. However, at the regional scale, the level of risk is lower due to their high green space coverage and low local temperature. This is consistent with the findings of Wu et al. (2023) at the city scale in the United States, which demonstrates that greenspace has positive mitigating effects on heat stress and contributes to HHR spatial heterogeneities to a certain extent.

The cross-scale analysis suggests that socioeconomic conditions

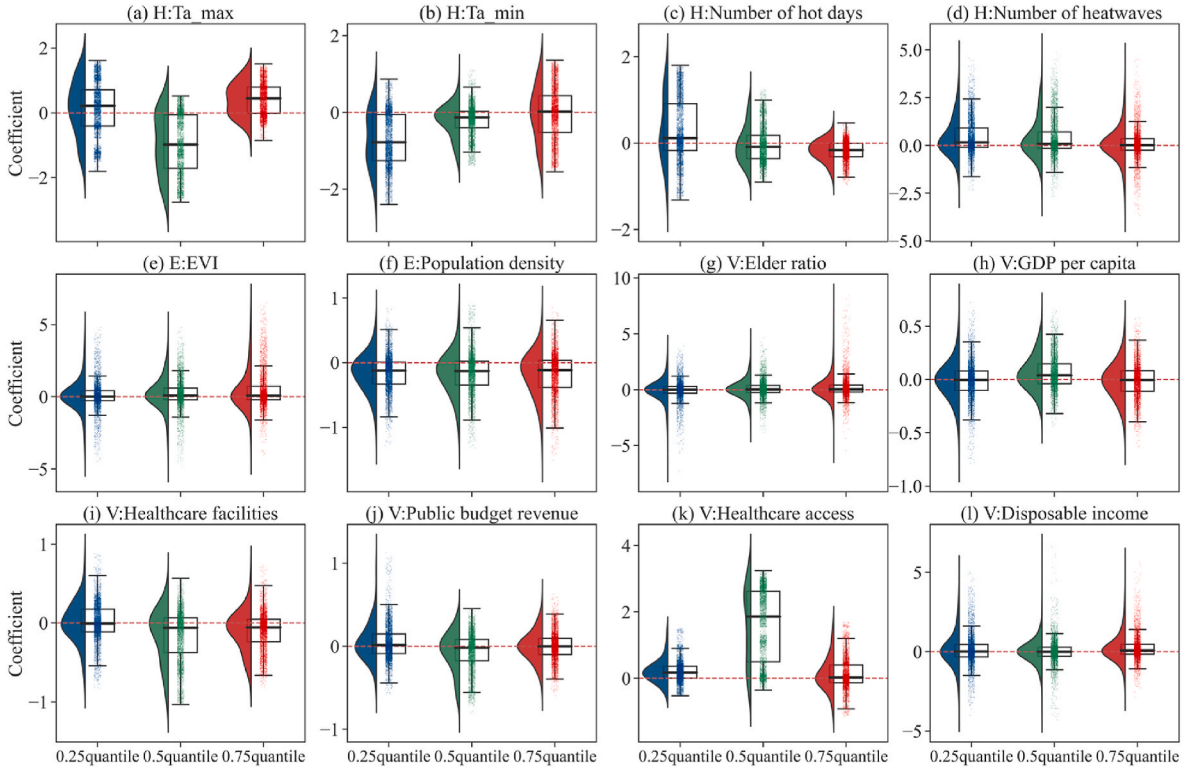

Fig. 7. Coefficient distribution of all HRI indicators at 0.25, 0.5, and 0.75 quantiles. The box plots show the distribution of all coefficients of indicators (95% CI). Blue, green, and red represent results at the 0.25, 0.5, and 0.75 quantiles, respectively. The dashed line is y = 0. All independent variables were standardized to 0–1. (For interpretation of the references to colour in this figure legend, the reader is referred to the Web version of this article.)

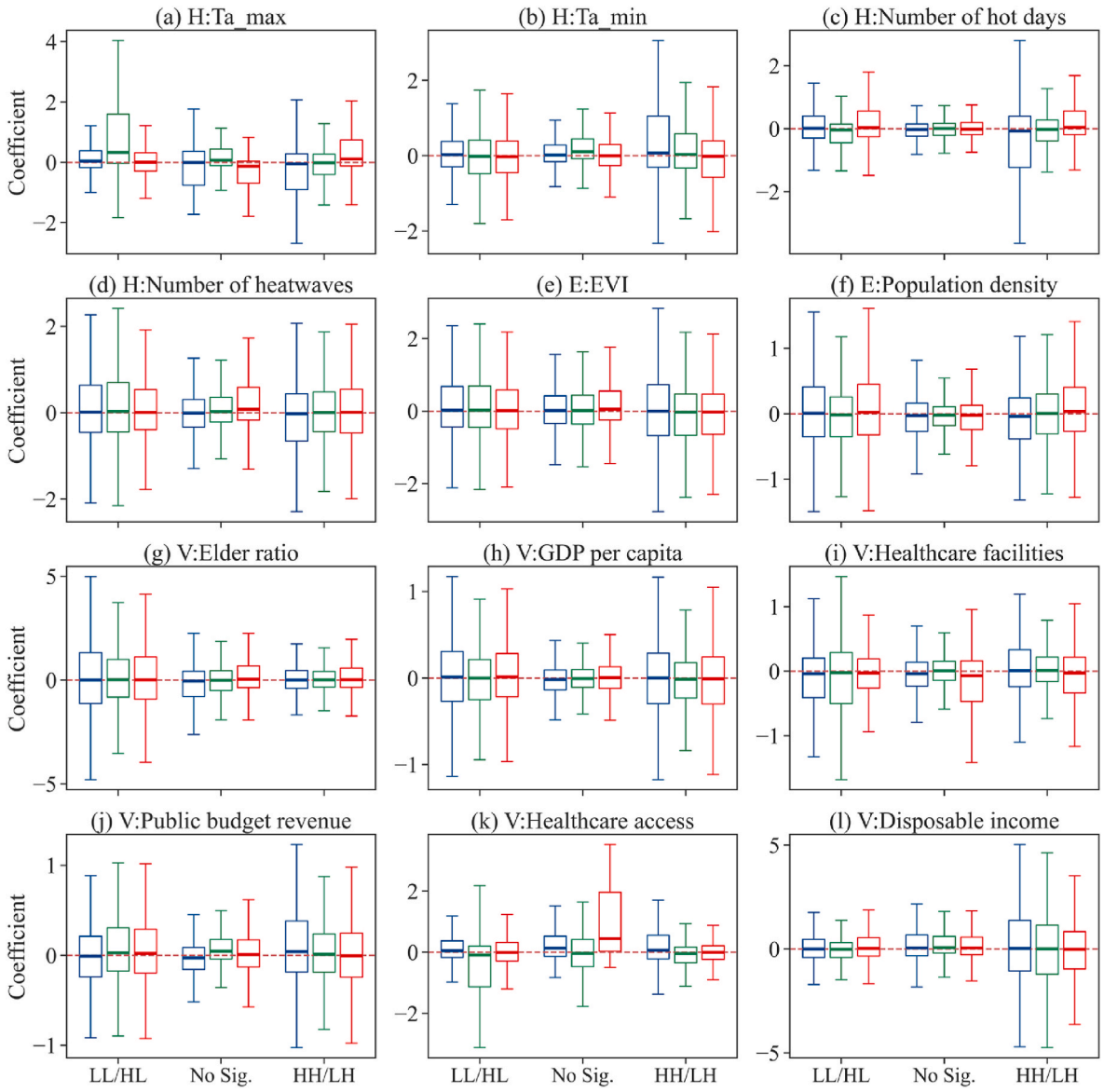

Fig. 8. Coefficient distribution of all HRI indicators in the different inequality level areas at 0.25, 0.5, and 0.75 quantiles. The box plots show the distribution of all coefficients of indicators (95% CI). Blue, green, and red represent results at the 0.25, 0.5, and 0.75 quantiles, respectively. The dashed line is y = 0. All independent variables were standardized to 0–1. (For interpretation of the references to colour in this figure legend, the reader is referred to the Web version of this article.)

contribute to the inequality of HHR in the YRD at the regional level. Environmental and socioeconomic status have a greater negative impact on regions with medium or low levels of inequality and a smaller impact on regions with high levels of equality. Due to the higher socioeconomic conditions, development in the region is more coordinated, and city residents are less vulnerable to heat stress. However, social and medical resources in less developed regions are mainly concentrated in urban areas, resulting in varying levels of exposure and resilience among residents. At the intra-regional scale, healthcare resource availability and the impact of localized temperatures are more significant, particularly in areas with low to moderate levels of HHR. In mega-city clusters, higher HHR caused by higher population concentrations and building density areas was often accompanied by lower intra-regional inequality due to high and coordinated socioeconomic levels. In areas of low and medium levels of risk, intra-regional healthcare resource availability and local temperatures have a greater impact on intra-regional inequities. This phenomenon may be unique to mega-city clusters.

The varying changes in spatial scales not only demonstrate the MAUP issue but also emphasize that different spatial scales capture different spatial processes. This highlights the necessity of examining risk inequality at multiple scales. A single spatial scale is insufficient for informing policy. Instead, different scales collectively define various areas that may be at risk of exposure to high temperatures and require possible interventions. It is important to note that inequality patterns vary with scale, which also determines people's behavioral patterns in the city. At the macroscale, people may migrate to other cities due to differences in temperature, regional income level, and socioeconomic conditions. At the mesoscale, residents may also migrate within a city due to differences in healthcare resources and living environments across different regions. This study can be used as a reference for studying the coupling between humans and cities in urban agglomeration systems at multiple scales. It is expected to generate more interest in the analysis of human health risks at different scales. The use of multi-scale analyses, ranging from macro to micro-environments, enables us to explore differences in risk across regions at a fine resolution, revealing more detailed spatial patterns than when using fixed single administrative boundaries.

4.4. Strategies to improve HHR equality in diverse regions

The multifaceted association between HHR inequality and its environmental and socioeconomic indicators indicates the need for improved HHR equality strategies. Since the problem of HHR is complicated by regional and intra-regional factors, it implies that policy decisions should also be multiscale. As the conceptual framework, we proposed in Fig. 9, the HHR inequality patterns could be divided based on the level of HHR at the regional scale and the level of HHR inequality within the regional scale.

Hence, these two dimensions delineate four quadrants of HHR inequality patterns that can be used for generating corresponding strategies to promote climate justice. Quadrant I, as the relative injustice and tough pattern, represents unequal and high HHR levels. Based on the results of sections 3.1 and 3.2, multiscale strategies would be needed for these regions, such as Quzhou and Jinhua. At the regional scale, the underdeveloped socioeconomic development and high concentration of population density are the main drivers. Regional cooperation and technological support from developed regions can be boosted to promote HHR equality at the regional scale. Additionally, within the regional scale, the unequal availability of healthcare facilities and high temperature may be the drivers of intra-regional inequality and socioeconomic development would be helpful to promote mesoscale HHR equality. Quadrant II is for unequal and low HHR pattern. The unequal pattern is dominant by the availability of healthcare facilities within the regional scale, which means more convenient and more balanced spatial distribution and planning of health facilities for residents would make these regions more just under urban heat threats. Whereas Quadrant III performs well in two dimensions, which is considered as the ideal pattern. It indicates that the residents here are exposed to equal and low distribution of HHR. In Quadrant IV, the region's equal and high HHR pattern represents that residents are equally exposed to high-level urban HHR such as Shanghai. Despite high socioeconomic levels and abundant healthcare resources, residents are still exposed to equally distributed but high HHR due to population overcrowding.

Like other urban clusters, the YRD has undergone significant land development and population growth in recent decades, which emphasizes the requirement for synergistic and sustainable development in the entire urban agglomeration. Solutions for high HHR areas vary depending on the inequality patterns. In Quadrant I, city administrators need to make more rational allocation and planning of public social resources such as increasing the equitable distribution of healthcare resources to reduce the intra-regional inequalities. Additionally, in Quadrant IV, it is important to increase the construction of fragmented green spaces due to the constraints of densely built environments while preserving the existing blue and green spaces (Guan et al., 2023; Venter et al., 2023). For quadrants II and III with low risk, it is necessary to preserve the existing natural environment and incorporate more equitable urban planning options into the urbanization process. At the same time, regional authorities should allocate resources at a macro-level to promote socio-economic development, including access to and quality of healthcare, especially in underdeveloped areas.

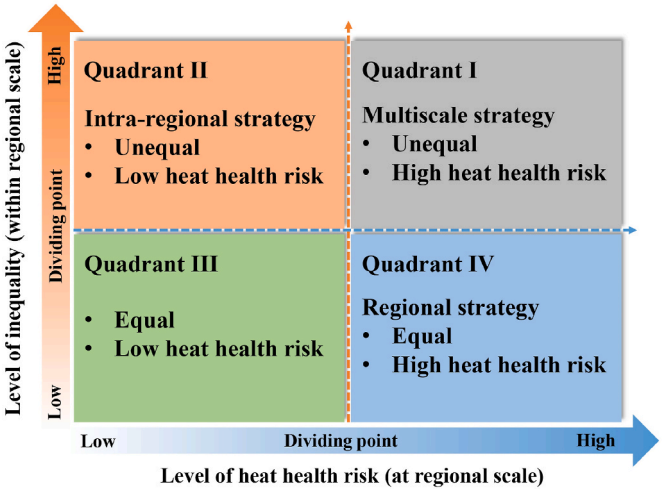

Fig. 9. Cross-scale HHR inequality patterns and corresponding strategies towards a more spatially equal development direction. Four HHR inequality patterns are divided based on two dimensions: level of heat health risk (x-axis) and level of inequality (y-axis). The level of inequality classifies regions according to the HHR inequality within the regional scale, whereas the level of heat health risk reflects the HRI values at the regional scale.

4.5. Limitations and outlook

This study also exhibits some limitations. First, in our multiscale study, we analyze risk inequality at macro, meso, and sub-meso (pixel grid) scales using Moran's I Index and Gini index. The indexes captured the overall state of risk equality between regions and their relationship with individual environmental and socioeconomic indicators. If reference heat-related morbidity and mortality data are available in the future, more comprehensive geospatial models that require dependent variables, such as multiscale GWR, can be considered to validate and improve the reliability of HHR assessment results. Therefore, the geospatial correlation index, such as the Getis-Ord G_i index, can be integrated to describe the multiscale HHR inequalities.

Additionally, we do not have a clear understanding of the effects of risk inequality at the micro-scale within each region, such as where it occurs and which neighborhoods or streets are affected by unfair risks (Renteria et al., 2022). There were two geospatial sampling processes involved in the calculation of HRI: upscaling (from high resolution to low resolution) and downscaling (the opposite). To capture the risk of inequality at the regional scale, we upscaled the fine data to 1 km, including NTL (from 100 m to 1 km), LULC (from 30 m to 1 km), and DEM (from 90 m to 1 km). Additionally, the socio-demographic statistical data were downscaled from the county level to 1 km to match with the raster data due to the restricted statistical caliber of the data, which is only available at the district and county level. However, this downscaling process ignored the spatial variations of the socio-demographic and economic inequalities within the region to some extent. In the future, multi-source geographic information data could be integrated to spatialize socio-demographic indicators related to heat vulnerability, providing finer spatial details.

Furthermore, spatial and statistical methods can be combined with community household-level survey analysis to explore populations that suffer from inequitable risk at the micro-scale (Petrović et al., 2022). For instance, White-Newsome et al. (2012) collected hourly indoor temperature measurements and building characteristics of 30 different homes in Detroit to examine the differences in residence temperatures. To measure personal exposure at the community or finer scale, it is important to consider finer characteristics such as building types (Gilabert et al., 2021; Kuras et al., 2017; Quinn et al., 2014).

Moreover, the use of regional-scale data in the quantitative framework for high-temperature risk and the factors for socioeconomic indicators in the factor analysis of equality impacts may be limited for more detailed equality analyses due to limited data availability (Niu et al., 2021). Qualitative but critical variables need to be considered and quantified in future research, including the underlying health condition, resident attitude and knowledge towards EHEs, and social cohesion effect on the elderly. In future research, multi-source data can be integrated, including cell phone signaling data and the spatialization of socioeconomic indicators. This will enable us to obtain finer-scale socioeconomic data at the community and street level, facilitating a more comprehensive analysis of inequality among residents at the micro-scale.

5. Conclusion

In this paper, we first quantified the HHR based on the multisource geo-information data and statistical data and then utilized the spatial autocorrelation method and statistical methods to examine the HHR inequality from macroscale to mesoscale. Moreover, we interpret the multifaceted relationship between HHR inequality with environmental and socioeconomic characteristics at and within the regional scale. Results showed that cities in YRD faced significant and unequal heat health risks, which presented a considerable challenge to protect people from heat stress and ensure equitable access to local heat mitigation measures at multiple scales. Specifically, higher HHR corresponding with higher population concentrations and building density areas are often accompanied by lower intra-regional inequality due to high and coordinated socioeconomic levels. Therefore, in areas with low and medium levels of risk, healthcare resource availability and local temperatures have a greater impact on intra-regional inequities, which vary at different levels of inequality.

Inequality levels of HHR at the regional scale reflect regional development and macroscale climate conditions, while mesoscale concentrations of HHR inequalities within regions are related to city-specific environmental and socioeconomic characteristics. Investigating and interpreting HHR inequalities at multiple scales is crucial as it can influence individual and regional development policies, as well as intra-regional social resource redistribution and social mechanisms. Based on cross-scale analysis, we propose strategies for addressing inequality with diverse patterns. Regional-level policies should consider that, in addition to within-city inequalities, there are significant disparities between cities. It is possible that an effective intervention in one city may not be effective in another, even if they are both located within the same region and in close proximity.

To the best of our knowledge, this is the first study to examine the multiscale HHR inequality and how its environmental and socioeconomic indicators affect inequality in different scales. Our findings showed that heat risk inequality varied and was influenced by different HHR indicators across different scales. Therefore, we suggested planning recommendations that can promote equality of HHR inequality at and within regional scales.

CRediT authorship contribution statement

Hanyi Wu: Writing – original draft, Software, Methodology, Investigation, Formal analysis, Data curation, Conceptualization. **Chuanwu Zhao:** Writing – review & editing, Visualization, Data curation. **Yu Zhu:** Writing – review & editing, Visualization, Data curation. **Yaozhong Pan:** Writing – review & editing, Supervision, Resources, Funding acquisition.

Declaration of competing interest

The authors declare that they have no known competing financial interests or personal relationships that could have appeared to influence the work reported in this paper.

Data availability

Data will be made available on request.

Acknowledgments

This research was funded by the National Natural Science Foundation of China (Grant No. 42192580, 42192581) and Open Fund of State Key Laboratory of Remote Sensing Science and Beijing Engineering Research Center for Global Land Remote Sensing Products (Grant No. OF202306). We thank the National Supercomputing Center in Zhengzhou, National Meteorological Data Center, European Mesoscale Weather Prediction Centre, U.S. Geological Survey, the National Aeronautics and Space Administration, Earth Remote Sensing Data Analysis Center of Japan, Department of Earth System Science of Tsinghua University, Open Street Map community and GaoDe map for providing data support for this study.

Appendix A. Supplementary data

Supplementary data to this article can be found online at https://doi.org/10.1016/j.jclepro.2024.142528.

References

Adams, R.M., Evans, C., Wolkin, A., Thomas, T., Peek, L., 2022. Social vulnerability and disasters: development and evaluation of a CONVERGE training module for researchers and practitioners. Disaster Prev. Manag. 31, 13–29. https://doi.org/10.1108/DPM-04-2021-0131.

Alizadeh, M.R., Abatzoglou, J.T., Adamowski, J.F., Prestemon, J.P., Chittoori, B., Akbari Asanjan, A., Sadegh, M., 2022. Increasing heat-stress inequality in a warming climate. Earth's Future 10, e2021EF002488. https://doi.org/10.1029/2021EF002488.

Beaudoin, M., Gosselin, P., 2016. An effective public health program to reduce urban heat islands in Québec, Canada. Rev. Panam. Salud Públic 40, 160–166.

Burke, M., Hsiang, S.M., Miguel, E., 2015. Global non-linear effect of temperature on economic production. Nature 527, 235–239. https://doi.org/10.1038/nature15725.

Cheng, W., Li, D., Liu, Z., Brown, R.D., 2021. Approaches for identifying heat-vulnerable populations and locations: a systematic review. Sci. Total Environ. 799, 149417 https://doi.org/10.1016/j.scitotenv.2021.149417.

Copernicus Climate Change Service (C3S), 2017. ERA5: Fifth Generation of ECMWF Atmospheric Reanalyses of the Global Climate.

Cutter, K.D., Susan, L., 2006. Crying wolf: repeat responses to hurricane evacuation orders. In: Hazards Vulnerability and Environmental Justice. Routledge, pp. 143–160.

Dialesandro, J., Brazil, N., Wheeler, S., Abunnasr, Y., 2021. Dimensions of thermal inequity: neighborhood social demographics and urban heat in the southwestern U. S. Int. J. Environ. Res. Publ. Health 18, 941. https://doi.org/10.3390/ijerph18030941.

Didan, K., 2015. MOD13A2 MODIS/terra vegetation indices 16-day L3 global 1km SIN grid V006. https://doi.org/10.5067/MODIS/MOD13A2.006.

Dorfman, R., 1979. A formula for the Gini coefficient. Rev. Econ. Stat. 146–149. https://doi.org/10.2307/1924845.

Ebi, K.L., Hess, J.J., 2020. Health risks due to climate change: inequity in causes and consequences. Health Aff. 39, 2056–2062. https://doi.org/10.1377/hlthaff.2020.01125.

Ellena, M., Melis, G., Zengarini, N., Di Gangi, E., Ricciardi, G., Mercogliano, P., Costa, G., 2023. Micro-scale UHI risk assessment on the heat-health nexus within cities by looking at socio-economic factors and built environment characteristics: the Turin case study (Italy). Urban Clim. 49, 101514 https://doi.org/10.1016/j.uclim.2023.101514.

Estoque, R.C., Ooba, M., Seposo, X.T., Togawa, T., Hijioka, Y., Takahashi, K., Nakamura, S., 2020. Heat health risk assessment in Philippine cities using remotely sensed data and social-ecological indicators. Nat. Commun. 11, 1581. https://doi.org/10.1038/s41467-020-15218-8.

Fernández, I.C., Wu, J., 2016. Assessing environmental inequalities in the city of Santiago (Chile) with a hierarchical multiscale approach. Appl. Geogr. 74, 160–169. https://doi.org/10.1016/j.apgeog.2016.07.012.

Gao, S., Xiong, Q., Yu, J., 2023. Conceptualization and measurement of water inclusive sustainability of China's cities in Yangtze River Economic Belt. Sustain. Cities Soc. 92, 104474 https://doi.org/10.1016/j.scs.2023.104474.

Gilabert, J., Deluca, A., Lauwaet, D., Ballester, J., Corbera, J., Llasat, M.C., 2021. Assessing heat exposure to extreme temperatures in urban areas using the Local Climate Zone classification. Nat. Hazards Earth Syst. Sci. 21, 375–391. https://doi.org/10.5194/nhess-21-375-2021.

Gong, P., Wang, J., Yu, L., Zhao, Yongchao, Zhao, Yuanyuan, Liang, L., Niu, Z., Huang, X., Fu, H., Liu, S., 2013. Finer resolution observation and monitoring of global land cover: first mapping results with Landsat TM and ETM+ data. Int. J. Rem. Sens. 34, 2607–2654. https://doi.org/10.1080/01431161.2012.748992.

Guan, J., Wang, R., Van Berkel, D., Liang, Z., 2023. How spatial patterns affect urban green space equity at different equity levels: a Bayesian quantile regression approach. Landsc. Urban Plann. 233, 104709 https://doi.org/10.1016/j.landurbplan.2023.104709.

He, B.-J., Zhao, D., Dong, X., Xiong, K., Feng, C., Qi, Q., Darko, A., Sharifi, A., Pathak, M., 2022. Perception, physiological and psychological impacts, adaptive awareness and knowledge, and climate justice under urban heat: a study in extremely hot-humid Chongqing, China. Sustain. Cities Soc. 79, 103685 https://doi.org/10.1016/j.scs.2022.103685.

He, C., Ma, L., Zhou, L., Kan, H., Zhang, Y., Ma, W., Chen, B., 2019. Exploring the mechanisms of heat wave vulnerability at the urban scale based on the application of big data and artificial societies. Environ. Int. 127, 573–583. https://doi.org/10.1016/j.envint.2019.01.057.

Hess, J., 2023. Heat and health inequity: acting on determinants of health to promote heat justice. Nat. Rev. Nephrol. 19, 143–144. https://doi.org/10.1038/s41581-023-00679-z.

Ho, H.C., Knudby, A., Huang, W., 2015. A spatial framework to map heat health risks at multiple scales. Int. J. Environ. Res. Publ. Health 12, 16110–16123. https://doi.org/10.3390/ijerph121215046.

Huang, H., Ma, J., Yang, Y., 2023. Spatial heterogeneity of driving factors for urban heat health risk in Chongqing, China: a new identification method and proposal of planning response framework. Ecol. Indicat. 153, 110449 https://doi.org/10.1016/j.ecolind.2023.110449.

Inostroza, L., Palme, M., Barrera, F. de la, 2016. A Heat Vulnerability Index: Spatial Patterns of Exposure, Sensitivity and Adaptive Capacity for Santiago de Chile. PLoS One 11, e0162464. https://doi.org/10.1371/journal.pone.0162464.

Justel, A., Peña, D., Zamar, R., 1997. A multivariate Kolmogorov-Smirnov test of goodness of fit. Stat. Probab. Lett. 35, 251–259. https://doi.org/10.1016/S0167-7152(97)00020-5.

Kim, Y.-J., Kim, B.-J., Shin, Y.-S., Kim, H.-W., Kim, G.-T., Kim, S.-J., 2019. A case study of environmental characteristics on urban road-surface and air temperatures during heat-wave days in Seoul. Atmosph. Ocean. Sci. Lett. 12, 261–269. https://doi.org/10.1080/16742834.2019.1608791.

Koks, E.E., Jongman, B., Husby, T.G., Botzen, W.J.W., 2015. Combining hazard, exposure and social vulnerability to provide lessons for flood risk management. Environ. Sci. Pol. 47, 42–52. https://doi.org/10.1016/j.envsci.2014.10.013.

Kuras, E.R., Richardson, M.B., Calkins, M.M., Ebi, K.L., Hess, J.J., Kintziger, K.W., Jagger, M.A., Middel, A., Scott, A.A., Spector, J.T., Uejio, C.K., Vanos, J.K., Zaitchik, B.F., Gohlke, J.M., Hondula, D.M., 2017. Opportunities and challenges for personal heat exposure research. Environ. Health Perspect. 125, 085001 https://doi.org/10.1289/EHP556.

Langlois, T.J., Fitzpatrick, B.R., Fairclough, D.V., Wakefield, C.B., Hesp, S.A., McLean, D. L., Harvey, E.S., Meeuwig, J.J., 2012. Similarities between line fishing and baited stereo-video estimations of length-frequency: novel application of kernel density estimates. PLoS One 7, e45973. https://doi.org/10.1371/journal.pone.0045973.

Lee, H., Kwon, H.-G., Ahn, S., Yang, H., Yi, C., 2023. Estimation of perceived temperature of road workers using radiation and meteorological observation data. Rem. Sens. 15, 1065. https://doi.org/10.3390/rs15041065.

Lee, S., Cho, Y.-I., Lee, M.-J., Lim, Y.-S., 2023. The evaluation of the temperature reduction effects of cool roofs and cool pavements as urban heatwave mitigation strategies. Appl. Sci. 13, 11451 https://doi.org/10.3390/app132011451.

Mitchell, B.C., Chakraborty, J., 2015. Landscapes of thermal inequity: disproportionate exposure to urban heat in the three largest US cities. Environ. Res. Lett. 10, 115005, 2020031315134572.

Mohajerani, A., Bakaric, J., Jeffrey-Bailey, T., 2017. The urban heat island effect, its causes, and mitigation, with reference to the thermal properties of asphalt concrete. J. Environ. Manag. 197, 522–538. https://doi.org/10.1016/j.jenvman.2017.03.095.

Mora, C., Dousset, B., Caldwell, I.R., Powell, F.E., Geronimo, R.C., Bielecki, C.R., Counsell, C.W.W., Dietrich, B.S., Johnston, E.T., Louis, L.V., Lucas, M.P., McKenzie, M.M., Shea, A.G., Tseng, H., Giambelluca, T.W., Leon, L.R., Hawkins, E., Trauernicht, C., 2017. Global risk of deadly heat. Nat. Clim. Change 7, 501–506. https://doi.org/10.1038/nclimate3322.

NASA/METI/AIST/Japan Spacesystems And U.S./Japan ASTER Science Team, 2009. ASTER global digital elevation model. https://doi.org/10.5067/ASTER/ASTGTM.002.

Niu, Y., Li, Z., Gao, Y., Liu, X., Xu, L., Vardoulakis, S., Yue, Y., Wang, J., Liu, Q., 2021. A systematic review of the development and validation of the heat vulnerability index: major factors, methods, and spatial units. Curr. Clim. Change Rep. 7, 87–97. https://doi.org/10.1007/s40641-021-00173-3.

Parry, M.L., 2007. Climate Change 2007-impacts, Adaptation and Vulnerability: Working Group II Contribution to the Fourth Assessment Report of the IPCC. Cambridge University Press.

Petrović, A., Manley, D., van Ham, M., 2022. Multiscale contextual poverty in The Netherlands: within and between-municipality inequality. Appl. Spatial Analys. 15, 95–116. https://doi.org/10.1007/s12061-021-09394-3.

Pianosi, F., Wagener, T., 2015. A simple and efficient method for global sensitivity analysis based on cumulative distribution functions. Environ. Model. Software 67, 1–11. https://doi.org/10.1016/j.envsoft.2015.01.004.

Pörtner, H.-O., Roberts, D.C., Tignor, M.M.B., Poloczanska, E., Mintenbeck, K., Alegría, A., Craig, M., Langsdorf, S., Löschke, S., Möller, V., Okem, A., Rama, B., 2022. IPCC 2022: Climate Change 2022 : Impacts, Adaptation and Vulnerability : Working Group II Contribution to the Sith Assessment Report of the Intergovernmental Panel on Climate Change (Report). Cambridge University Press, Cambridge, UK.

Quinn, A., Tamerius, J.D., Perzanowski, M., Jacobson, J.S., Goldstein, I., Acosta, L., Shaman, J., 2014. Predicting indoor heat exposure risk during extreme heat events. Sci. Total Environ. 490, 686–693. https://doi.org/10.1016/j.scitotenv.2014.05.039.

Renteria, R., Grineski, S., Collins, T., Flores, A., Trego, S., 2022. Social disparities in neighborhood heat in the Northeast United States. Environ. Res. 203, 111805 https://doi.org/10.1016/j.envres.2021.111805.

Román, M.O., Wang, Z., Sun, Q., Kalb, V., Miller, S.D., Molthan, A., Schultz, L., Bell, J., Stokes, E.C., Pandey, B., Seto, K.C., Hall, D., Oda, T., Wolfe, R.E., Lin, G., Golpayegani, N., Devadiga, S., Davidson, C., Sarkar, S., Praderas, C., Schmaltz, J., Boller, R., Stevens, J., Ramos González, O.M., Padilla, E., Alonso, J., Detrés, Y., Armstrong, R., Miranda, I., Conte, Y., Marrero, N., MacManus, K., Esch, T., Masuoka, E.J., 2018. NASA's Black Marble nighttime lights product suite. Rem. Sens. Environ. 210, 113–143. https://doi.org/10.1016/j.rse.2018.03.017.

Shamsaei, M., Carter, A., Vaillancourt, M., 2022. A review on the heat transfer in asphalt pavements and urban heat island mitigation methods. Construct. Build. Mater. 359, 129350 https://doi.org/10.1016/j.conbuildmat.2022.129350.

Song, J., Yu, H., Lu, Y., 2021. Spatial-scale dependent risk factors of heat-related mortality: a multiscale geographically weighted regression analysis. Sustain. Cities Soc. 74, 103159 https://doi.org/10.1016/j.scs.2021.103159.

Sun, Y., Li, Y., Ma, R., Gao, C., Wu, Y., 2022. Mapping urban socio-economic vulnerability related to heat risk: a grid-based assessment framework by combing the geospatial big data. Urban Clim. 43, 101169 https://doi.org/10.1016/j.uclim.2022.101169.

Sun, Y., Xie, S., Zhao, S., 2019. Valuing urban green spaces in mitigating climate change: a city-wide estimate of aboveground carbon stored in urban green spaces of China's Capital. Global Change Biol. 25, 1717–1732. https://doi.org/10.1111/gcb.14566.

Todeschi, V., Pappalardo, S.E., Zanetti, C., Peroni, F., Marchi, M.D., 2022. Climate justice in the city: mapping heat-related risk for climate change mitigation of the urban and Peri-urban area of Padua (Italy). ISPRS Int. J. Geo-Inf. 11, 490. https://doi.org/10.3390/ijgi11090490.

Venter, Z.S., Figari, H., Krange, O., Gundersen, V., 2023. Environmental justice in a very green city: spatial inequality in exposure to urban nature, air pollution and heat in Oslo, Norway. Sci. Total Environ. 858, 160193 https://doi.org/10.1016/j.scitotenv.2022.160193.

Wan, Z., Hook, S., Hulley, G., 2015. MOD11A1 MODIS/terra land surface temperature/emissivity daily L3 global 1km SIN grid V006. https://doi.org/10.5067/MODIS/MOD11A1.006.

Wang, S., Sun, Q.C., Huang, X., Tao, Y., Dong, C., Das, S., Liu, Y., 2023. Health-integrated heat risk assessment in Australian cities. Environ. Impact Assess. Rev. 102, 107176 https://doi.org/10.1016/j.eiar.2023.107176.

Wang, W., Zeng, J., Li, X., Liao, F., Zhang, T., Yin, F., Deng, Y., Ma, Y., 2024. Using a novel strategy to identify the clustered regions of associations between short-term exposure to temperature and mortality and evaluate the inequality of heat- and cold-attributable burdens: a case study in the Sichuan Basin, China. J. Environ. Manag. 349, 119402 https://doi.org/10.1016/j.jenvman.2023.119402.

White-Newsome, J.L., Sánchez, B.N., Jolliet, O., Zhang, Z., Parker, E.A., Timothy Dvonch, J., O'Neill, M.S., 2012. Climate change and health: indoor heat exposure in vulnerable populations. Environ. Res. 112, 20–27. https://doi.org/10.1016/j.envres.2011.10.008.

Wong, M.S., Peng, F., Zou, B., Shi, W.Z., Wilson, G.J., 2016. Spatially analyzing the inequity of the Hong Kong urban heat island by socio-demographic characteristics. Int. J. Environ. Res. Publ. Health 13, 317. https://doi.org/10.3390/ijerph13030317.

Wu, H., Xu, Y., Zhang, M., Su, L., Wang, Y., Zhu, S., 2024. Spatially explicit assessment of the heat-related health risk in the Yangtze River Delta, China, using multisource remote sensing and socioeconomic data. Sustain. Cities Soc. 104, 105300 https://doi.org/10.1016/j.scs.2024.105300.

Wu, S., Yu, W., Chen, B., 2023. Observed inequality in thermal comfort exposure and its multifaceted associations with greenspace in United States cities. Landsc. Urban Plann. 233, 104701 https://doi.org/10.1016/j.landurbplan.2023.104701.

Xu, X., Xu, Z., Chen, L., Li, C., 2019. How does industrial waste gas emission affect health care expenditure in different regions of China: an application of bayesian quantile regression. Int. J. Environ. Res. Publ. Health 16, 2748. https://doi.org/10.3390/ijerph16152748.

Zhang, W., Zheng, C., Chen, F., 2019. Mapping heat-related health risks of elderly citizens in mountainous area: a case study of Chongqing, China. Sci. Total Environ. 663, 852–866. https://doi.org/10.1016/j.scitotenv.2019.01.240.

Zhong, S., Qian, Y., Zhao, C., Leung, R., Wang, H., Yang, B., Fan, J., Yan, H., Yang, X.-Q., Liu, D., 2017. Urbanization-induced urban heat island and aerosol effects on climate extremes in the Yangtze River Delta region of China. Atmos. Chem. Phys. 17, 5439–5457. https://doi.org/10.5194/acp-17-5439-2017.

Zhu, W., Yuan, C., 2023. Urban heat health risk assessment in Singapore to support resilient urban design — by integrating urban heat and the distribution of the elderly population. Cities 132, 104103. https://doi.org/10.1016/j.cities.2022.104103.